International Journal of Thermophysics, Vol. 26, No. 4, July 2005 (© 2005)
DOI: 10.1007/s10765-005-6683-y

Electrostatic Levitation Research and Development at JAXA: Past and Present Activities in Thermophysics[1]

P.-F. Paradis,[2,3] T. Ishikawa,[2] and S. Yoda[2]

This paper reviews the past and present research and development activities in the field of electrostatic levitation at the Japan Aerospace Exploration Agency (JAXA). Particular emphasis is given on the important innovations of sub-millimeter sample handling, launch levitation initiation, aero-electrostatic hybrid levitation, multi-beam heating geometry, electrode design, and ultraviolet (UV) imaging. A summary of the thermophysical properties of refractory materials measured in their liquid states, above and below their melting point, as well as preliminary results of samples solidified from deep supercooled states are also reported.

KEY WORDS: ceramics; levitation; liquid; metal; semiconductor; solidification; supercooling; thermophysical property.

1. INTRODUCTION

To support materials and fluids science experiments in microgravity, it is necessary to counter g-jitters and external forces (optical, aerodynamic, etc.) imparted to bodies under study and to position accurately a sample in space and time. This requirement triggered a host of hardware development, all of which have their own merits and limitations [1–13].

Early efforts to electrostatically levitate millimeter-size objects were pursued by the German Aerospace Center (DLR) [1]. In particular, processing of a glass forming ceramic was attempted during a sounding rocket

[1] Paper presented at the Seventh International Workshop on Subsecond Thermophysics, October 6–8, 2004, Orléans, France.

[2] Japan Aerospace Exploration Agency, Tsukuba Space Center, 2-1-1 Sengen, Tsukuba, Ibaraki, 305-8505 Japan.

[3] To whom correspondence should be addressed. E-mail: paradis.paulfrancois@jaxa.jp

0195-928X/05/0700-1031/0 © 2005 Springer Science+Business Media, Inc.

flight using a tetrahedral electrode configuration [2]. Ground-based technology demonstrators, using several electrode configurations (tetrahedral, parallel plates, rings, etc.) and operational under vacuum as well as atmospheric conditions, were successfully developed later at the Jet Propulsion Laboratory [3, 7]. Besides sample positioning, fundamental development in areas of rotation [14, 15] and oscillation control [16] was achieved for various materials (e.g., H_2O, metals (Sn, Si, Ti, Zr), metallic alloys (NiZr, glass forming), Si). This opened unique research opportunities in drop dynamics [17], property measurements (density [18], C_p/ε_T [19], surface tension, viscosity [16]), and solidification studies [20]. More recently, solidification of a ceramic under reduced-gravity experiments was carried out on-board a sounding rocket by the National Space Development Agency of Japan [13].[4] Although several successes were obtained, both the ground and the space hardware showed limitations and problems with respect to handling of sub-millimeter samples, time needed to reach the liquid state, type of material processed (no glass-forming ceramics reported), sample position instability due to anisotropic evaporation and photon pressure, and luminosity of molten refractory materials (led to erroneous density and C_p/ε_T data with negative effect on derived quantities (surface tension and viscosity)).

This paper first reviews the important technological innovations contributed to the field of electrostatic levitation by the Japan Aerospace Exploration Agency (JAXA). It then presents a summary of the main scientific results obtained in the fields of thermophysical-property measurements of refractory materials at high temperatures (liquid and supercooled states), solidification from the supercooled phase, and atomic structure.

2. JAXA TECHNOLOGICAL INNOVATIONS

To take advantage of a microgravity environment, JAXA wanted to establish a containerless facility for the International Space Station to process and study glass and ceramics under pressurized atmospheres in addition to elemental metals, metallic alloys, and semiconductors in vacuum [21, 22]. However, before this could be achieved, ground-based research was initiated to solve the problems of sample handling, processing time, type of processed material, and luminosity. Scientific objectives included the physical and structural property measurements of liquid materials above as well as under their melting point, the understanding of

[4] The National Space Development Agency (NASDA) merged with the National Aeronautical Laboratory and the Institute of Space and Astronautical Science on October 1, 2003 to become the Japan Aerospace Exploration Agency (JAXA).

metastable phase formation, vitrification, diffusion, and the synthesis of novel materials.

2.1. Handling of Sub-millimeter Sample [21, 22]

Early designs of electrostatic levitators used a carousel below the bottom electrode for sample handling [23]. This worked fine for hard samples with diameters larger than 1.5 mm but jamming problems arose for smaller samples or for soft materials. In addition, with a single pedestal being used, a risk of contamination was possible if samples of different materials were processed. Fig. 1a shows, among other things, the sample handling mechanism used with the JAXA vacuum electrostatic levitator. It consists of a single sliding cartridge containing ten individual molybdenum or tungsten pedestals. Not only does this circumvent any cross-talk contamination problems between distinct samples but permits the handling of very soft or porous materials. Sub-millimeter samples can also be easily handled using this system thus avoiding any jamming problems. A conical catcher helps to retrieve unsuccessfully levitated samples. Fig. 1b shows the hybrid pressurized aero-electrostatic levitator for which sample loading is from the top, also allowing the handling of porous, soft, non-spherical, and sub-millimeter samples.

2.2. Electrode Configuration of the Levitator and Coils

The parallel disk electrode design, together with the four surrounding spherical electrodes reported early in the development of electrostatic levitators [7], provided sufficient lateral stability for many materials (Sn, Zr, Si, etc.). However, the horizontal restoring forces supplied by this scheme are not strong enough when dealing with evaporative materials (Ti, Mo, V, etc.). Sample instability problems are acute especially when large laser power is used to reach extreme temperatures. In JAXA studies, samples with diameters from 0.9 to 3 mm, charged by electronic emission, were levitated one at the time between two horizontal electrodes: a concave bottom electrode (30 mm dia.) and a flat, smaller top electrode (10 mm dia.) with a through-hole (Fig. 1a). The conical electrical field distribution resulting from this arrangement provided a horizontal field component and thus a natural restoring force towards the center. The bottom electrode was made out of tungsten to withstand severe temperatures. A field between 4 and 20 kV and a feedback loop (720 Hz) ensured that the sample was maintained in a fixed position. The feedback relied on a PID scheme, identical to that reported earlier [3] and implemented by two sets of orthogonally disposed He–Ne lasers and position sensors (Fig. 2a, b). This, together

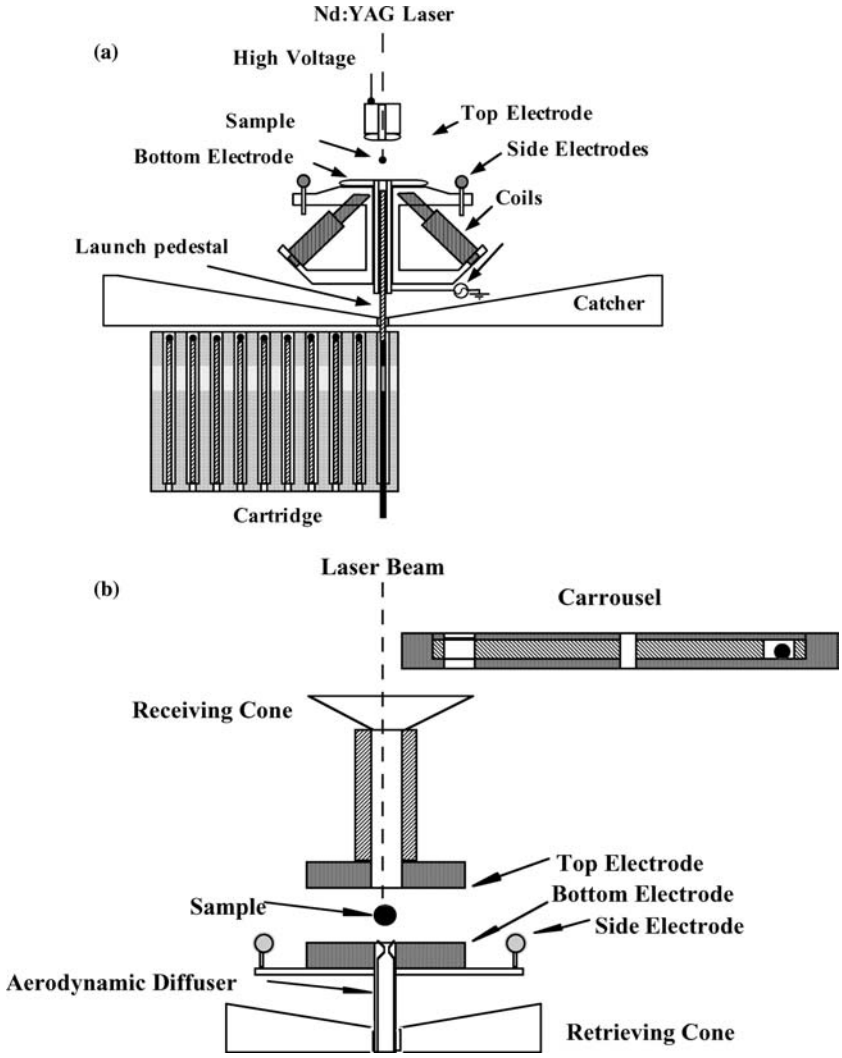

Fig. 1. Schematic diagram showing electrodes design and sample handling system for (a) the vacuum electrostatic levitator and (b) for the hybrid aerodynamic-electrostatic levitator.

with four spherical electrodes at the height of a levitated sample, offered improved three-dimensional (3-D) sample stability, even for high vapor-pressure materials.

Following earlier work [15], four coils were used as a stator to generate a horizontal and rotating magnetic field. Each coil was wound on

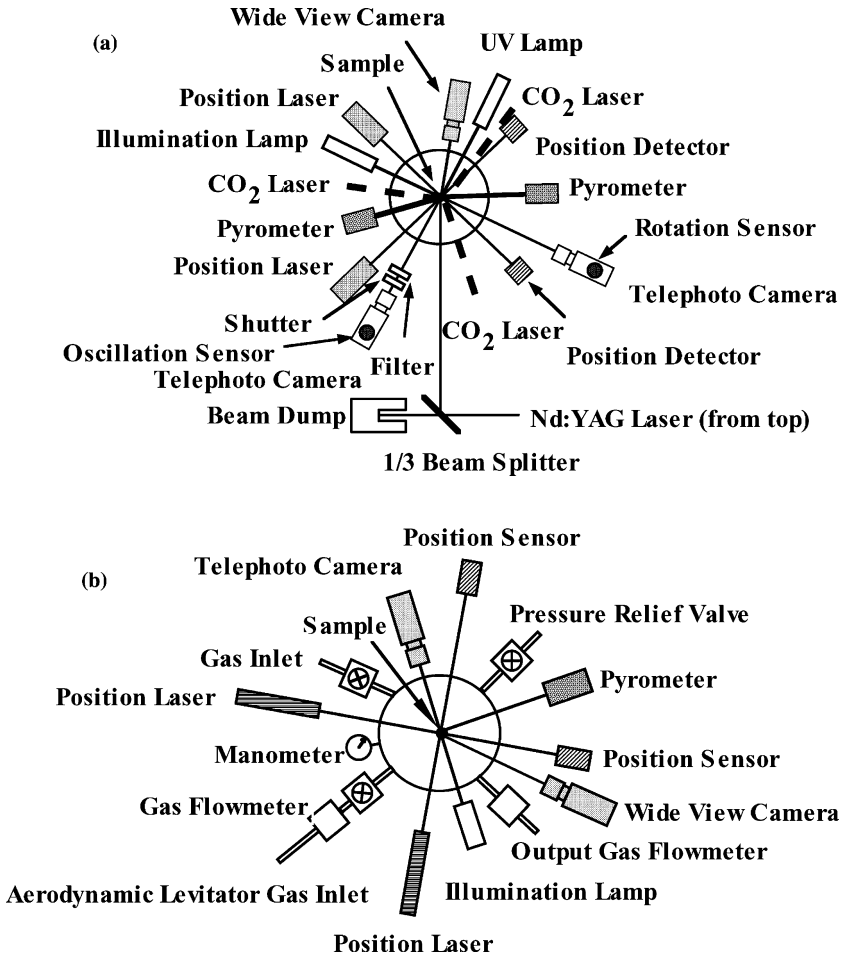

Fig. 2. Schematic diagram showing chamber layout and laser heating configuration for (a) the vacuum electrostatic levitator (Note that a 1/3 beam splitter is sometimes used (e.g. Ta, Re) with a beam dump to increase the range of applicability of the Nd:YAG laser) and (b) the hybrid aerodynamic-electrostatic levitator.

a glass spool with insulated copper wire. The glass was used to electrically insulate the spools from the proximity of the high voltage electrode. A soft iron core was inserted in the spool to increase the magnetic field. In our facility, the coils surrounded the lower electrode. This geometry was selected as it helped maintenance and diminished the risk of arcing between the high voltage top electrode and the coils. Plates of Macor^{TM}

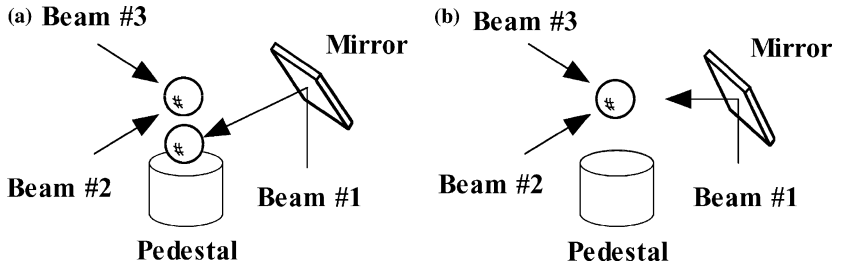

Fig. 3. Schematic diagram showing the launch initiation technique [25].

further prevented any arcing and protected the coil assembly from contact with an unsuccessfully processed molten sample.

Processing was carried out in an $\sim 10^{-5}$ Pa vacuum for metals and semiconductors and under a 450 kPa atmosphere (N_2, air) for ceramics. For ceramics, the pedestal was replaced with an aerodynamic levitator (Fig. 1b) [24].

2.3. Hot Launch Levitation Initiation [25]

The time required to bring samples of some materials into the liquid state, for which characterization is intended, can take several hours due to electrical charge loss occurring upon heating if photoelectric effect charging alone is used [23]. To alleviate this problem, a sample, resting on the pedestal, was heated with one laser beam while two remaining beams converged at the location at which the sample was going to be positioned after the launch (Fig. 3a) [26]. Once the sample reached a temperature close to 1500 K, at which the thermionic emission was sufficient to charge the sample, the high voltage between the two electrodes was applied and the feedback control software was activated. A few seconds later, the sample was launched into its normal levitation position and the pre-heating laser beam was redirected on the sample to ensure position stability (Fig. 3b). This technique is easily applied to materials with melting temperature higher than 1500 K. However, samples of lower melting point materials have a tendency to stick on the pedestal and can be contaminated.

With the hybrid facility, a single beam from the system described above was used and the power was adjusted to maintain a constant temperature during the different launch initiation stages. The aerodynamic levitator offered containerless conditions, overcame sample stickiness, and allowed sample charging prior to launch into electrostatic mode [24]. The containerless conditions make it possible to initiate levitation of molten

or near-molten samples without any risk of contamination. Using this preheating technique, the liquid state could be reached within a few minutes.

2.4. Multi-beam Heating Geometry [26, 27]

To avoid the destabilizing effect of photon and evaporative anisotropic induced forces [26] and to maintain good stability for samples processed under vacuum, while observing the constraint of the chamber layout, a flattened tetrahedral laser heating configuration was implemented (Figs. 1a and 2a) [27]. Three focused beams (50 W each) of CO_2 lasers (10.6 μm emission) in a same plane, separated by 120 degrees, hit the specimen. In addition, the focused beam of a 500 W Nd:YAG laser (1.064 μm) heated the sample from the top. Heating with the most powerful laser along the vertical was the best configuration as the strongest field and the fastest feedback were also along this axis. Besides the exceptional 3-D sample-position stability, this multi-beam heating configuration helped to control sample rotation and improved the temperature homogeneity.

The radiance temperature was measured by pyrometry and was calibrated to true temperature using the known melting plateau of the material. The emissivity found from the pyrometer at the melting point was kept constant over the entire liquid and undercooled regions. It is important to note that recent measurements with a fast polarimeter revealed variations in the emissivity of the liquid phase of several metals [28]. Usually, the emissivity decreased with an increase of temperature. Unfortunately, such data for undercooled metals have not been reported yet but it is plausible that a similar phenomenon occurs. Fig. 4 depicts a typical temperature profile for a levitated tungsten sample after the laser beams have been turned off. A 500 K undercooling and a sudden temperature rise due to the release of the latent heat of fusion upon solidification is observed.

2.5. Ultraviolet (UV) Imaging [25]

Early determination of density using the technique described in Ref. 18 led to erroneous data when applied to molten refractory materials (e.g., W, Re, Ta) due to the large blackbody output variation in the optical region. Because the blackbody output of a sample from say, 1500 to 4000 K does not vary much in the ultraviolet, a CCD video camera equipped with a low-pass filter (450 nm) in conjunction with a high intensity UV background light [25] was used. Fig. 5 shows the imaging of a Zr sample at different temperatures (300, 1500, and 2500 K from left to right)

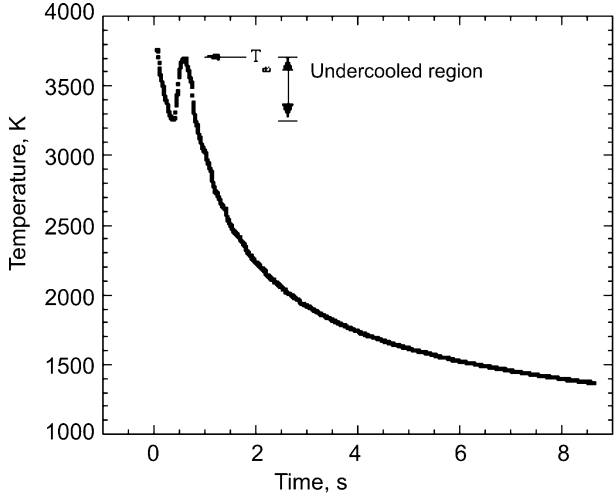

Fig. 4. Temperature profile of a heated and radiatively cooled W sample showing supercooling and recalescence.

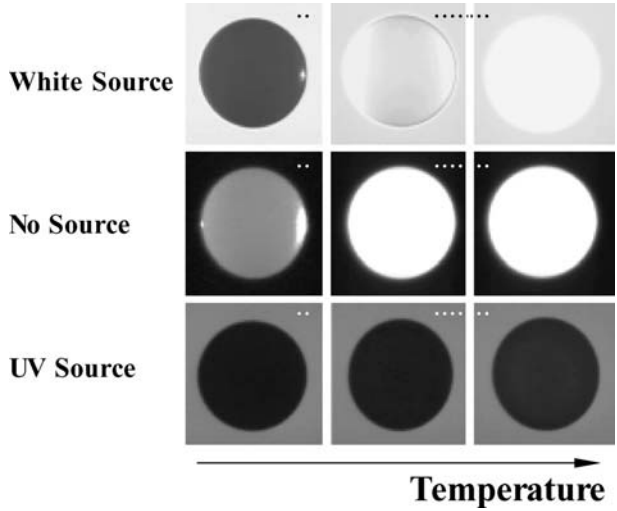

Fig. 5. Effect of the background on the appearance of a sample at several temperature [25].

for no background (a, b, c), a white-light background illumination (d, e, f), and a UV background illumination (g, h, i). As shown in the figure, the UV illumination offered a contrast between sample and background

practically independent of the sample temperature. This scheme permitted accurate determinations of the density and the vapor pressure [25, 29].

2.6. Vapor Pressure [29]

The sample area variation in time could be accurately measured for a given temperature using the UV imaging technique, knowing the elapsed time between the start and the end of an experiment. Since the sample evaporated isotropically, the effusion Knudsen method [30] could be utilized assuming that the effective area of effusion A was the surface of the sample at a given time. Therefore, the vapor pressure V_p (Pa) could be found using the equation [29],

$$V_p(T) = 1.013 \times 10^5 (m/(tA))[2\pi \mathrm{R} T M]^{1/2} \quad (1)$$

where m/t is the measured rate of evaporation in vacuo, R is the universal gas constant, T is the sample temperature, and M is the molar mass.

3. EXPERIMENTAL RESULTS

3.1. Thermophysical-Property Measurements

The high melting temperature of refractory materials and the risk of contamination at elevated temperature make it difficult to measure the properties of the liquid phase using traditional methods. This explains why density and surface-tension data are so scarce and mainly limited to the melting point and why no viscosity data appear in the literature for elemental metals with melting points above 2504 K. Over the years, several measurements were systematically performed at JAXA to fill the void for this important class of materials. Here is presented a summary of the thermophysical property measurements (density, vapor pressure, surface tension, viscosity) of refractory materials above as well as below their melting points.

3.1.1. Density [27, 31–47]

The density was determined by simultaneously recording the temperature and images of a non-rotating spherical sample illuminated from behind with a UV source. Upon closing the shutters of all lasers, the sample was cooled and the data could be obtained over a large temperature range. The sample area was extracted from each digitized video image and matched to a temperature profile. These images were calibrated by levitating a sphere of precisely known diameter under identical conditions. Since the sample was axi-symmetric and because its mass was known, the

Table I. Density of Various Materials in their Liquid Phase

Material	T_m (K)	$\rho(T_m)$ (kg $\cdot m^{-3}$)	Temperature coeff. ($kg \cdot m^{-3} \cdot K^{-1}$)	Temperature (K)	Reference
W	3695	17400	−0.94	3175 – 3690	[47]
Re	3453	18400	−0.91	2700 – 3810	[27]
Ta	3269	15000	−0.41	2760 – 3580	[27]
Mo	2896	9099	−0.60	2500 – 3000	[34]
Nb	2742	7727	−0.39	2340 – 2900	[31]
Ir	2720	19500	−0.85	2300 – 3000	[46]
Ru	2607	10750	−0.56	2225 – 2775	[45]
Hf-3 (Wt.%) Zr	2504	12000	−0.44	2220 – 2875	[44]
B	2360	2160	−0.19	2150 – 2500	[43]
Rh	2236	10821	−0.76	1820 – 2250	[36]
V	2183	5460	−0.49	1840 – 2240	[33]
Zr	2128	5980	−0.93	1800 – 2400	[32]
Ti	1943	4100	−0.99	1750 – 2050	[32]
Pd	1828	10660	−0.77	1640 – 1875	[42]
Ni	1728	7890	−0.65	1420 – 1850	[41]
Si	1683	2548	$-0.16(T-T_m)$ -1.28×10^{-4} $(T-T_m)^2$	1350 – 1820	[39]
Al_2O_3	2327	2930	−0.12	2175 – 2435	[40]
$Y_3Al_5O_{12}$	2240	4080	−0.29	1470 – 2420	[38]
Nd-$CaAl_2O_4$	1878	3070	−0.11	1570 – 2000	[35]
$BaTiO_3$	1893	4040	−0.34	1300 – 2025	[37]
$BiFeO_3$	1363	6740	−1.31	1250 – 1490	[37]

density could be found for each temperature by dividing the mass by the volume. In these measurements, the uncertainty was estimated to be less than 2% from the resolution of the video grabbing capability (640×480 pixels) and from the uncertainty in mass measurement (± 0.0001 g). Optical microscopy and electron probe microanalysis were performed to ensure that voids or oxide or nitride layers were not present on the surface or in the bulk of the solidified samples. The data measured so far are summarized in Table I and Fig. 6. At the melting point, our value agrees generally very well with the values published in the literature [48]. Except for the quadratic behavior exhibited by Si (agrees with Ref. 49), the linear dependence with temperature compares well with the theoretical works of Reynolds [50] and Steinberg [51]. To our knowledge, many of these measurements were the first to be reported that included a large temperature excursion into the supercooled region.

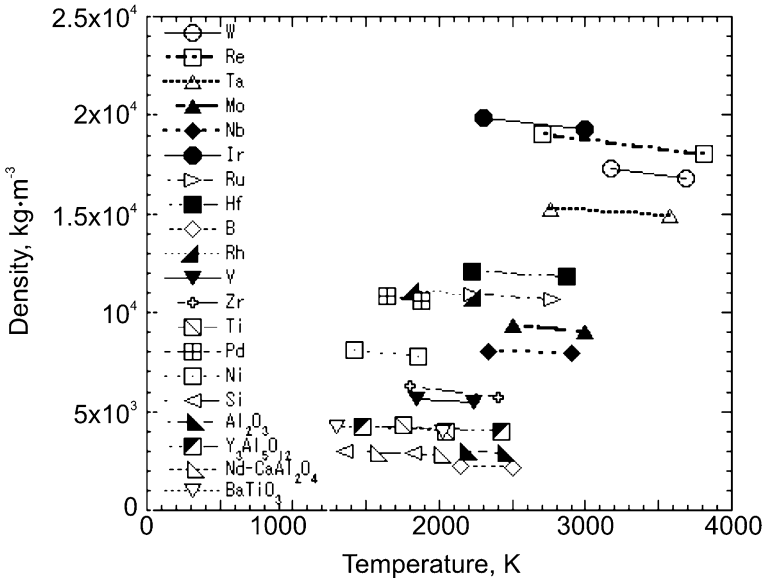

Fig. 6. Density of several liquid and supercooled materials versus temperature.

3.1.2. Vapor Pressure [29]

With the excellent sample position stability offered by the facility, a molten Ti sample could be levitated long enough ($\gg 15$ min.) for vapor-pressure data to be taken using the method introduced earlier [29]. The vapor pressure, $V_p(T)$(Pa), could be fitted by

$$\log V_p(T) = 9.154 - 17978T^{-1} \quad (1700\text{–}2050\,K). \tag{2}$$

Extrapolating the data to T_m, our datum compared rather well with those obtained elsewhere when respective uncertainties are considered [29]. The observed discrepancy could be accounted for by the lower binding energy experienced by the atoms of our liquid sample compared with that of the solid samples used in other studies. Although this technique is attractive to investigate corrosive liquids, severe coating of the windows of the chamber occurring during the continuous heating of evaporative materials over a long period made its application a little bit cumbersome and expensive.

3.1.3. Surface Tension and Viscosity [44–47, 52–54]

The surface tension and viscosity were determined by studying the behavior of the sample oscillation about its equilibrium shape [55]. In this technique [16, 56], a sample was first heated, melted, and brought to a

selected temperature. A $P_2\cos(\theta)$-mode drop oscillation was then induced to the sample by superimposing a small sinusoidal electric field on the levitation field. The transient signal that followed the termination of the excitation field was detected and analyzed. This was done several times at a given temperature and repeated over a large temperature range. Using the characteristic oscillation frequency of the signal after correcting for non-uniform surface charge distribution [57], the surface tension can be found. Similarly, the viscosity was obtained using the decay time of the same signal. For these measurements, real-time values of the radius and density data were used to prevent any distortion in the measured properties due to sample evaporation. The uncertainty of the measurements was estimated to be better than 5% from the response of the oscillation detector and from the density measurements.

The surface tension and viscosity measurements were taken over large temperature ranges, well above the melting temperature and down into the supercooled region. A list of the data measured over the years by JAXA is presented in Tables II and III. The surface tension, like that of other pure metals, exhibited a linear behavior as a function of temperature (Fig. 7). At the melting point, our values show remarkable agreement with most published values [48] and our temperature coefficients compare generally well with those calculated by Allen [58]. Moreover, by using our density data at the melting point, the $T_m/V_m^{2/3}$ factor ($V_m^{2/3}$ being the quotient of the molar mass over density) could be calculated and, together with our surface tension value at the melting point, shows excellent agreement with the empirical relation proposed by Reynolds et al. [50]. The viscosity data for the investigated metals are extremely scarce, and besides Zr, are limited to the melting point. Our data nonetheless compare well with the scarce data appearing in the literature when experimental uncertainties are considered. Furthermore, even when no data are available in the literature (Ti, Nb, Ru, Ir, Mo, Ta, Re, W) our data at T_m generally agree well with the calculated values by Andrade [59]. The temperature dependence of the viscosity exhibited an Arrhenius behavior for all measured metals (Fig. 8).

From all the data for the refractory materials, it seems remarkable that other than their very high melting temperatures, the magnitude of their properties or the behavior of their temperature dependence are not significantly different from those of lower melting point materials, even when compared with mercury at 300 K.

The measured thermophysical properties of several refractory metals with 4d and 5d electrons (Ti, Zr, Hf, Nb) were compared with calculations based on the hard sphere (HS) model. Despite rough assumptions such as rectangular density of state, and the determination of packing fractions and

Table II. Surface Tension of Various Metals

Material	T_m (K)	$\sigma(T_m)$ (mN·m^{-1})	Temperature coeff. (mN·m^{-1}·K^{-1})	Temperature (K)	Reference
W	3695	2365	−0.17	3350–3700	[47]
Re	3453	2710	−0.23	2800–3600	[54]
Ta	3290	2154	−0.21	3150–3400	[53]
Mo	2896	2262	–	2896	–
Ir	2720	2230	−0.17	2373–2833	[46]
Ru	2607	2260	−0.24	2450–2725	[45]
Nb	2742	1937	−0.20	2320–2915	[52]
Hf-3(Wt.%) Zr	2504	1614	−0.10	2220 – 2675	[44]
Rh	2236	1935	−0.30	1850 – 2400	[36]
Zr	2128	1500	−0.11	1800 – 2400	[52]
Ti	1943	1557	−0.16	1750 – 2050	[52]
Ni	1728	1739	−0.22	1553 – 1963	[41]

Table III. Viscosity of Various Metals

Material	T_m(K)	$\eta(T_m)$ (mPa·s)	Temperature coeff. (mPa·s·K^{-1})	Temperature (K)	Reference
W	3695	6.8	0.108 $e^{[128000/RT]}$	3350 – 3700	[47]
Re	3453	8.0	0.079 $e^{[133000/RT]}$	2900 – 3600	[54]
Ta	3290	8.6	0.0035 $e^{[213/RT]}$	3150 – 3400	[53]
Mo	2896	6.0	–	2896	–
Ir	2720	6.9	1.85 $e^{[30000/RT]}$	2373 – 2773	[46]
Ru	2607	6.1	0.60 $e^{[49800/RT]}$	2450 – 2725	[45]
Nb	2742	4.50	0.553 $e^{[4885/RT]}$	2320 – 2915	[52]
Hf-3 (Wt.%) Zr	2504	5.13	0.495 $e^{[48650/RT]}$	2220 – 2675	[44]
Rh	2236	1.97	0.090 $e^{[64300/RT]}$	1850 – 2400	[36]
Zr	2128	4.74	0.033 $e^{[76640/RT]}$	1800 – 2300	[52]
Ti	1943	4.42	0.763 $e^{[31810/RT]}$	1750 – 2050	[52]
Ni	1728	7.4	0.07 $e^{[67000/RT]}$	1553 – 1963	[41]

plasma parameters, agreement between measured and calculated values is reasonably good [60].

3.2. Atomic Structure Characterization by Neutron Scattering Experiments [61, 62]

A vacuum electrostatic levitation furnace was developed for the structural study of materials above the melting point as well as in the supercooled phase by neutron scattering. Preliminary experiments done

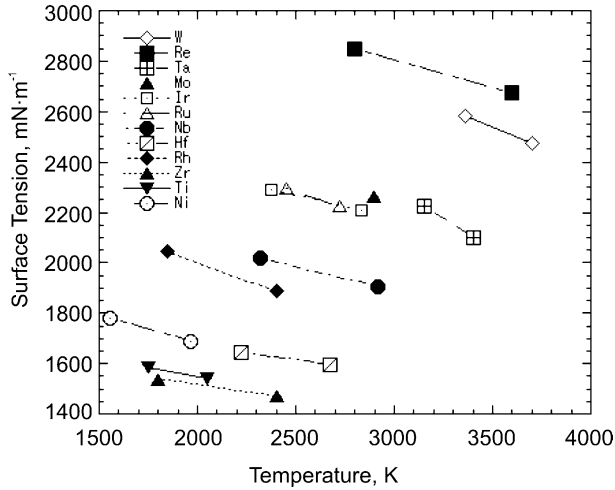

Fig. 7. Surface tension of several liquid and supercooled materials versus temperature.

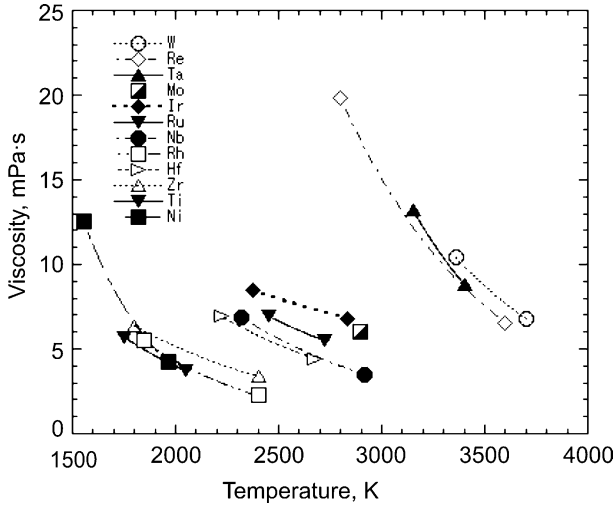

Fig. 8. Viscosity of several liquid and supercooled materials versus temperature.

using the high resolution powder diffractometer (HRPD) at the Advanced Science Research Center of the Japan Atomic Energy Research Institute with a solid alumina sample did not reveal any sharp peaks in the background data coming from the furnace materials. This is an advantage compared to other methods for which parts of the levitators generate

sharp peaks [63-65]. The observed diffraction peak intensities and location were identified as those derived from the mirror indices of hexagonal structure of alumina and were in complete agreement with those reported in the literature [66]. Preliminary experiments to investigate the structure of liquid zirconium are currently underway. A similar facility is currently under development for the structural study of liquids by *X*-ray scattering.

3.3. Processing and Solidification from Supercooled Phases [67, 68]

Besides elemental metals, several compounds such as Nd–$CaAl_2O_4$, $CaAl_2O_4$, $Y_3Al_5O_{12}$, Al_2O_3, CaF_2, 76%BaB_2O_4–24%Na_2O, BaB_2O_4, YIG, some slags, $BiFeO_3$, $BaTiO_3$, and $Nd_2Fe_{14}B$ have been processed using either the pressurized or vacuum facilities. It was possible to vitrify Nd–$CaAl_2O_4$, $CaAl_2O_4$, $Y_3Al_5O_{12}$, and BaB_2O_4compositions from the supercooled state.

The containerless solidification behavior of $\sim$2 mm diameter $Nd_2Fe_{14}B$ samples was studied at different cooling rates and the effects of supercooling depth on the microstructure and magnetization were investigated [67]. For the sample solidified at the lower supercooling level, the developed dendritic residual Fe and Nd rich phases were found in the microstructure. For the sample solidified with the higher supercooling level, the developed dendritic Fe was suppressed and a fine microstructure was obtained (average grain size of $Nd_2Fe_{14}B$: $\sim$2–4 μm). Furthermore, the sample that experienced the deeper supercooling had a higher magnetization than that of the sample processed with a lesser degree of supercooling.

Solidification of barium titanate ($BaTiO_3$) from deep supercooled phases at different cooling rates was carried out with the pressurized levitation furnace. In addition, the material resulting from containerless solidification was transparent and consisted of micrometer-size particles and a single crystal phase exhibiting a giant dielectric constant over 100000 and a weak temperature dependence over the 300–100 K range [68]. Future work is currently under progress to develop with a model and a theory to explain the results.

4. CONCLUSIONS

Electrostatic levitation is a wonderful approach (spherical samples, maintain deep undercooling, large observation) for the characterization and study of materials and shows promise for the synthesis of novel materials. However, it is still in its infancy. As far as processing is concerned, the technique has been mainly used with metals and a better knowledge of the charging mechanisms is essential to permit systematic levitation of

ceramics. Because the hot launch technique cannot be used for low melting temperature materials in vacuum, and although the UV photoelectric charging scheme works, it is very time consuming. Ways to improve charging either by using shorter wavelength sources such as table top *X*-ray lasers or by cleaning the surface by atomic beams could alleviate this shortcoming.

Property measurements would also benefit from several improvements and additions to the current techniques. The density measurement technique is quite mature but a further improvement might allow resolving the changes in the liquid density due to the structural changes occurring in some liquid-phase transitions of glass forming materials. The use of VUV or *x*-ray sources as a background to the sample would offer improved imaging, in particular, for samples near 4000 K. The surface tension and viscosity data obtained so far are remarkable in a sense that they provided measurements unknown before, and that now, extend all the way to tungsten (> 4000 K). However, rather large scatter appears in the viscosity data due to the motion of the sample upon exciting the drop oscillation as the feedback control system tends to bring back a perturbed sample to its original position. This issue will need to be addressed for more precise experiments to be possible. Moreover, since the electrostatic scheme did not input any heat, a high temperature sample in vacuum experienced pure radiative cooling when the heating sources are shut off. From the simplification of the energy equation governing the cooling, the ratio of the constant pressure heat capacity and hemispherical total emissivity could be determined. Independent ways to measure either the hemispherical total emissivity or the isobaric heat capacity (e.g., by adding a drop calorimeter to the levitator) are currently sought.

Although several successes were achieved with the ground-based electrostatic levitation furnaces, difficulties were faced when handling iron, certain alloys, and oxides due to insufficient charges before reaching the melting point. Microgravity conditions would allow levitation of these materials or larger samples while providing a quiet environment. This would facilitate solidification studies of oxides and alloys as well as property measurements of materials of vital industrial importance (e.g., Fe, Ge) [69]. However, some questions remain about how easy the surface tension measurement in microgravity would be. This is because the drop charge (needed to calculate the surface tension [16]) is determined by the levitation conditions, which involve the gravitational acceleration, which, in turn, virtually disappears in microgravity.

Over the last few years, a strong focus was placed on thermophysical-property measurements of refractory materials, in particular elemental metals (W, Re, Ta, etc.). In the future, emphasis will gradually shift

towards property measurements of industrial ceramic and metallic alloys. Specifically, ways to implement surface tension and viscosity measurement techniques of ceramics to the pressurized aero-electrostatic levitation furnace and precise electrical resistivity of metals will be investigated. Parallel efforts will be devoted to the atomic structure characterization of liquid and supercool melts by neutron as well as synchroton radiation scattering.

ACKNOWLEDGMENTS

The authors would like to thank Dr. W.-K. Rhim (California Institute of Technology) and Dr. J.K.R. Weber (Containerless Research Inc.) for several fruitful and challenging discussions over the years. The authors are also grateful to Y. Saita (Advanced Engineering Services) for help in some experiments.

REFERENCES

1. P. F. Clancy, E. G. Lierke, R. Grossbach, and W. M. Heide, *Acta Astron.* **7**:877 (1980).
2. E. G. Lierke, R. Grossbach, G. H. Frischat, and K. Fecker, *ESA SP-1132* **1**:370 (1991).
3. W.-K. Rhim, M. Collender, M. T. Hyson, W. T. Simms, and D. D. Elleman, *Rev. Sci. Instrum.* **56**:307 (1985).
4. C. S. Ray and D. E. Day, *Mater. Res. Soc. Symp. Proc.* **87**:239 (1987).
5. G. Sridharan, *Rev. Sci. Instrum.* **61**:2251 (1990).
6. D. M. Herlach, R. F. Cochrane, I. Egry, H. J. Fecht, and A. L. Greer, *Mater. Rev.* **38**:273 (1993).
7. W.-K. Rhim, S.-K. Chung, D. Barber, K.-F. Man, G. Gutt, A. Rulison, and R. E. Spjut, *Rev. Sci. Instrum.* **64**: 2961 (1993).
8. J. K. R. Weber, D. S. Hampton, D. R. Merkley, C. A. Rey, and M. M. Zatarski, *Rev. Sci. Instrum.* **65**:456 (1994).
9. F. Babin, J.-M. Gagné, P.-F. Paradis, J.-P. Coutures, and J.-C. Rifflet, *Micro-g. Sci. Tech.* **7**:283 (1995).
10. P.-F. Paradis, F. Babin, and J.-M. Gagné, *Rev. Sci. Instrum.* **67**:262 (1996).
11. J. Guigné, S. Koplenko, V. Chin, S. Whelan, M. Barmatz, and H. W. Jackson, *Micro-g. Sci. Tech.* **7**:290 (1995).
12. A. A. Rulison, J. L. Watkins, and B. Zambrano, *Rev. Sci. Instrum.* **68**:2856 (1997).
13. S. Yoda, N. Koshikawa, T. Nakamura, J. Yu, T. Nakamura, Y. Nakamura, S. Yoshitomi, H. Karasawa, T. Ikeda, Y. Arai, M. Kobayashi, Y. Awa, H. Shimoji, T. Morita, and S. Shimada, *J. Jpn. Soc. Microg. Appl.* **17**:76 (2000).
14. W.-K. Rhim and P.-F. Paradis, *Rev. Sci. Instrum.* **70**:4652 (1999).
15. W.-K. Rhim and T. Ishikawa, *Rev. Sci. Instrum.* **69**:3628 (1998).
16. W.-K. Rhim, K. Ohsaka, P.-F. Paradis, and R. E. Spjut, *Rev. Sci. Instrum.* **70**:2796 (1999).
17. W.-K. Rhim, S.-K. Chung, and D. D. Elleman, *ESA SP*-295, 629 (2001).
18. S.-K. Chung, D. B. Thiessen, and W.-K. Rhim, *Rev. Sci. Instrum.* **67**:3175 (1996).
19. A. A. Rulison and W.-K. Rhim, *Rev. Sci. Instrum.* **65**:695 (1994).
20. K. Ohsaka, S. K. Chung, and W.-K. Rhim, *Appl. Phys. Lett.* **70**:423 (1997).

21. P.-F. Paradis, T. Ishikawa, and S. Yoda, *ESA SP-454*, 993 (2001).
22. T. Ishikawa, P.-F. Paradis, and S. Yoda, *J. Jpn. Soc. Microg. Appl.* **18**:106 (2001).
23. W.-K. Rhim, private communication, Jet Propulsion Laboratory, Pasadena, California (1998).
24. P.-F. Paradis, T. Ishikawa, J. Yu, and S. Yoda, *Rev. Sci. Instrum.* **72**:2811 (2001).
25. T. Ishikawa, P.-F. Paradis, and S. Yoda, *Rev. Sci. Instrum.* **72**:2490 (2001).
26. P.-F. Paradis, T. Ishikawa, and S. Yoda, *Space Technol.* **22**:81 (2002).
27. P.-F. Paradis, T. Ishikawa, and S. Yoda, *Appl. Phys. Lett*. **83**:4047 (2003).
28. C. Cagran, C. Brunner, A. Seifter, and G. Pottlacher, *High Temp.- High Press.* **34**:669 (2002).
29. P.-F. Paradis, T. Ishikawa, and S. Yoda, *European J. Phys. Appl. Phys.* **22**:97 (2003).
30. M. Knudsen, *Ann Physik*. **28**:75 (1909).
31. P.-F. Paradis, T. Ishikawa, and S. Yoda, *J. Mater. Sci.* **36**:5125 (2001).
32. T. Ishikawa, P.-F. Paradis, and S. Yoda, 2nd Pan-Pacific Basin Workshop on Microgravity Sciences, TP-1019, Pasadena, California (May, 2001), p. 180.
33. P.-F. Paradis, T. Ishikawa, T. Aoyama, and S. Yoda, *J. Chem. Thermodyn.* **34**:1929 (2002).
34. P.-F. Paradis, T. Ishikawa, and S. Yoda, *Int. J. Thermophys.* **23**:555 (2002).
35. P.-F. Paradis, J. Yu, T. Ishikawa, and S. Yoda, *J. Am. Ceram. Soc.* **86**:2234 (2003).
36. P.-F. Paradis, T. Ishikawa, and S. Yoda, *Int. J. Thermophys.* **24**: 1121 (2003).
37. P.-F. Paradis, J. Yu, T. Ishikawa, T. Aoyama, and S. Yoda, *Appl. Phys. A* **76**:1965 (2004).
38. P.-F. Paradis, J. Yu, T. Ishikawa, T. Aoyama, S. Yoda, and J. K. R. Weber, *J. Cryst. Growth* **249**:523 (2003).
39. P.-F. Paradis, T. Ishikawa, and S. Yoda, *J. Japan Soc. Microg. Appl.* **20**:218 (2003).
40. P.-F. Paradis, T. Ishikawa, Y. Saita, and S.Yoda, *Jpn. J. Appl. Phys.* **43** (4A):1496 (2004).
41. T. Ishikawa, P.-F. Paradis, and S. Yoda, *J. Jpn. Inst. Met.* **68**:101 (2004).
42. P.-F. Paradis, T. Ishikawa, and S. Yoda, *Int. J. Thermophys.* **25**:1905 (2004).
43. P.-F. Paradis, T. Ishikawa, and S. Yoda, *Appl. Phys. Lett*. **86**:151901 (2005).
44. P.-F. Paradis, T. Ishikawa, and S. Yoda, *Int. J. Thermophys.* **24**:239 (2003).
45. P.-F. Paradis, T. Ishikawa, and S. Yoda, *J. Mater. Res.* **19**:590 (2004).
46. T. Ishikawa, P.-F. Paradis, and S. Yoda, *Int. J. Thermophys.* (in press).
47. P.-F. Paradis, T. Ishikawa, and S. Yoda, *Appl. Phys. Lett.* **86**:41901 (2005).
48. D. R. Lide and H. P. R. Frederikse, eds., *CRC Handbook of Chemistry and Physics*, 78th Ed. (CRC Press, Boca Raton, Florida, 1997).
49. W.-K. Rhim, S.-K. Chung, A. A. Rulison, and R. E. Spjut, *Int. J. Thermophys.* **18**:459 (1997).
50. C. L. Reynolds, P. R. Couchman, and F. E. Karasz, *Philos. Mag.* **34**:659 (1976).
51. D. J. Steinberg, *Metall. Trans.* **5**: 1341 (1974).
52. P.-F. Paradis, T. Ishikawa, and S. Yoda, *Int. J. Thermophys.* **23**:825 (2002).
53. P.-F. Paradis, T. Ishikawa, and S. Yoda, *J. Appl. Phys.* **97**:053506 (2005).
54. T. Ishikawa, P.-F. Paradis, and S. Yoda, *Appl. Phys. Lett.* **85**:5866 (2004).
55. Lord Rayleigh, *Proc. R. Soc. London* **14**:184 (1882).
56. S. Sauerland, G. Lohöfer, and I. Egry, *J. Non Cryst. Solids* **156–158**:833 (1993).
57. J. Q. Feng and K. V. Beard, *Proc. R. Soc. London* **A 430**:133 (1990).
58. B. C. Allen, Trans. *AIME* **227**:1175 (1963).
59. E. N. Andrade, *Phil. Mag.* **17**:698 (1934).
60. T. Ishikawa, P.-F. Paradis, T. Itami, and S. Yoda, *J. Phys. Chem.* **118**:7912 (2003).
61. P.-F. Paradis, T. Ishikawa, and S. Yoda**,** *J. Non-Cryst. Solids* **312–314**:309 (2002).
62. H. Aoki, P.-F. Paradis, T. Ishikawa, T. Aoyama, T. Masaki, S. Yoda, Y. Ishii, and T. Itami**,** *Rev. Sci. Instrum.* **74**:1147 (2003).

63. C. Landron, X. Launay, J.-C. Rifflet, P. Echegut, Y. Auger, D. Ruffier, J.-P. Coutures, M. Lemonier, M. Gailhanou, M. Bessiere, D. Bazin, and H. Dexpert, *Nucl. Instrum. Meth. Phys. Res. B* **124**:627 (1997).
64. S. Ansell, S. Krishnan, J. K. R. Weber, J. J. Felten, P. C. Nordine, M. A. Beno, D. L. Price, and M.-L. Saboungi, *Phys. Rev. Lett.* **78**:464466 (1997).
65. G. Jacobs and I. Egry, *Phys. Rev. B* **59**:3961 (1999).
66. T. C. Huang, W. Parrish, N. Masciocchi, and P. W. Wang, *Adv. X-ray Anal.* **33**:295 (1990).
67. J. Yu, P.-F. Paradis, T. Ishikawa, S. Ozawa, T. Saito, T. Motegi, and S. Yoda, *Jpn J. Appl. Phys.* **41**:2908 (2002).
68. J. Yu, P.-F. Paradis, T. Ishikawa, and S. Yoda, *Appl. Phys. Lett.* **85**:2899 (2004).
69. H. Fecht, *THERMOLAB* – European Projects for Thermophysical Properties Thermophys Project (2000).